IEEE Access
Multidisciplinary | Rapid Review | Open Access Journal

Received May 9, 2018, accepted June 6, 2018, date of publication June 19, 2018, date of current version July 12, 2018.

Digital Object Identifier 10.1109/ACCESS.2018.2848903

Measurement-Based Modeling of a Semitransparent CdTe Thin-Film PV Module Based on a Custom Neural Network

YASMEEN HUSSEIN SABRY[1,2], W. Z. W. HASAN[1], (Member, IEEE), A. H. SABRY[1], MOHD ZAINAL ABIDIN AB KADIR[1], (Senior Member, IEEE), M. A. M. RADZI[1], (Member, IEEE), AND S. SHAFIE[1]

[1]Department of Electrical and Electronics Engineering, Faculty of Engineering, Universiti Putra Malaysia, Serdang 43400, Malaysia
[2]Ministry of Electricity, Baghdad, Iraq

Corresponding authors: W. Z. W. Hasan (wanzuha@upm.edu.my) and A. H. Sabry (ahs4771384@gmail.com)

This work was supported by the Department of Electrical and Electronics Engineering, Universiti Putra Malaysia, under Grant 9515302.

ABSTRACT Semitransparent photovoltaic (STPV) can be employed in a wide application range to provide sunlight permeability for supplying solar electrical energy with some shading, which is preferable in hot areas. To predict the output power and formulate the performance of this type of photovoltaic (PV) system, the proposed approach analyzes a Thin-Film solar cadmium telluride-type module and develops a custom neural network (CNN) for modeling its generated power expressed by its mathematical formula. Experiments for single and multilayer installation topologies are conducted for performance analysis. The coefficients of the model equation are investigated based on a set of power-current curves. The developed model adopts three factors: a minimum number of hidden neurons, the use of all measured data to train the network weights, and a linear output activation function to reduce the complexity of solving the network equations. The results specify the limit at which this type of PV starts generating power from the experimental measurements and the comparison with its equivalent normal PV module. The CNN-based STPV module is verified by comparing with the experimental measurements results, which shows a reasonable R-square, while its performance is evaluated on the silicon-based PV by comparing its behavior with the two-diode model PV in the MATLAB-based simulation.

INDEX TERMS Artificial neural network, modeling, measurements, semitransparent PV.

I. INTRODUCTION

The rapid evolution of PV as an alternative means of energy generation is bringing it closer to making a significant contribution to addressing the challenges posed by the rapid growth of worldwide energy demand and associated environmental issues. Together with the main existing technology, which is based on silicon (Si), the growth of this field is intertwined with the development of new materials and fabrication methods [1]. Thin-Film solar cells based on cadmium telluride (CdTe) are complex devices that have great potential for achieving high conversion efficiencies [2]. Improvements in the performance of Thin-Film solar cells need to be accelerated. Although some energy conversion losses are inevitable, the origins of the remaining electrical and optical losses and corresponding solutions need to be clearly identified for Thin-Film PV technologies. Many photovoltaic (PV) devices exhibit poor performance in the field (i.e., actual use conditions). A significant part of this loss of performance is due to variations in sunlight [3].

Recently, semitransparent photovoltaic (STPV) systems have been employed in a wide application range as resources to supply solar electrical energy with some sunlight permeability and shading. The generated electricity represents a major advantage over movable shading devices for adjusting the transmitted sunlight. Available commercial STPV modules comprise encapsulated crystalline/silicon PV cells between two layers of glass or a transparent plastic film. The energy efficiency improvement and the high utilization of renewable energy are important targets for sustainable green energy productions. Few experimental measurements of such PV types have been carried out. In a greenhouse application, the installation of two STPV prototypes in the greenhouse roof and the annual attained electrical energy for the greenhouse land area showed that these modules could be sufficient for such applications in high irradiation areas [4]. Thin-Film and organic STPV technologies are now being adopted as low-cost solutions for greenhouse applications because of their power generation and transparent, flexible

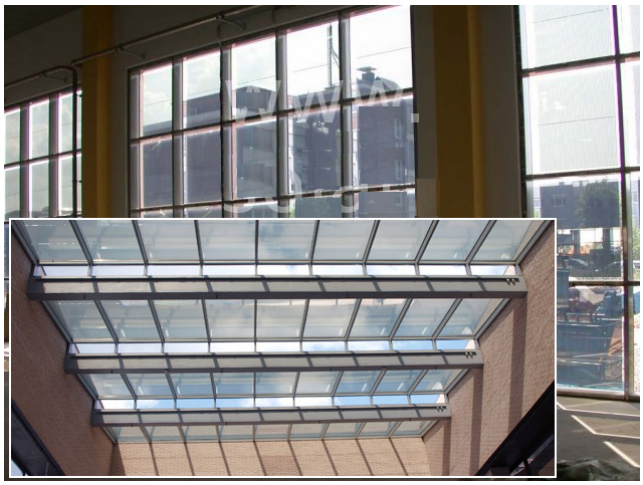

FIGURE 1. Building Integrated Photovoltaic.

properties [5]. For organic and Thin-Film STPV modules, the transparency replaces the normal PV area ratio to express the sunlight amount that is interspersed through the glazing. Their main drawback is that they cannot generate power on cloudy days or in winter. Building Integrated Photovoltaic (BIPV) is a new type of building material, which provides green energy as well as building preservation as in FIGURE 1. Apart from generating electricity, BIPV modules can be customized in a different dimension, thickness, shape, and color [6].

Literature models predict the I–V characteristic of a PV system as a function of irradiance, angle of incidence of solar radiation, the spectrum of sunlight, and temperature [7]. For the last few years, a substantial amount of work has been performed to develop simulation models and extract model parameters of photovoltaic (PV) systems [7]–[10]. The PV model plays an important role in the accuracy of the time simulation of the PV cell model. Modeling of the PV cell involves the estimation of the I–V and P–V characteristic curves to emulate the real cell under various environmental conditions. This performance assessment will aid an understanding of the I–V curves for forecasting PV system output power under inconsistent input conditions [11].

Mathematical modeling of solar cells is essential for any operation yield optimization. In general, the PV module is represented by an equivalent circuit in which the parameters are calculated using the experimental current-voltage characteristic. These parameters are generally quantities that are neither measurable nor included in the manufacturing data. As a consequence, they must be determined from the systems of the I-V equations (current-voltage) for diverse points of a function given by the manufacturer or from direct measurements on the module [12]. Modeling and simulation of PV modules would help provide a better understanding of their behavior and characteristics. These methods can be effectively used to predict the variations in the behavior of the PV module with environmental conditions [13]–[15]. Some data are required to predict a solar panel's generated power. However, such data might not be available due to a lack of related databases [16]. The artificial neural network (ANN) has widely used for solar data prediction [17]. The harvested energy for single or multiple panels is relatively accepted compared with the equivalent silicon-based solar panel and can be improved by considering the tilt angle in the installation process. Since the solar tracker has the ability to track the sun even on overcast days, in contrast to a fixed-tilted PV system, it could be efficient during practical weather conditions over the year, which include a sequential mixture of sunny, cloudy and overcast days [18]. Along with the weather data, the sun's positional variations during the day were also taken into account. Finally, four models using linear regression, logarithmic regression, polynomial regression, and ANN were constructed [19]. Several analytical modeling techniques based on complex mathematical expressions for estimating the behavior of solar cells have been reported in the literature. Several models for solar cells utilize non-linear lumped parameter equivalent circuits, and their parameters are determined by experimental current-voltage characteristics using analytical or numerical extraction techniques [20], [21].

A Comparison table summarizes the common and the similarities between the proposed and the previous related works can be listed in Table 1, where the proposed work recognized with a dark color to show the common points with other related work in the same color.

In PV measurements, there is a lack of information about the power pattern, efficiency, and limitations of Thin-Film PV modules. Moreover, it is not clear if the power modeling of Thin-Film PV modules provides information that can help PV system users identify the daily energy that can be harvested from this multi-purpose product or avoid potential degradation of power.

The key contributions of this paper are as follows:

- customizing the ANN architecture to synthesize its topology for providing an output formula through solvable nonlinear algebraic equations. This is accomplished by; acquiring data with a high rate of sampling, normalizing the data set, selecting one hidden layer with no more than 6 neurons and a non-linear activation function, and using output neurons with linear activation function.
- Predicting the output power and formulate the performance of a PV system with mathematical equations derived from the proposed CNN.
- Proposing an approach analyzes a Thin-Film solar cadmium telluride (CdTe)-type module and developing a model for its behavior.

In this paper, we present a modeling approach for the STPV module based on custom neural network (CNN) and extract the power formula of such system. The key objectives of this research are to analyze, model and simulate Thin-Film PV modules under different installation topologies and under uneven row shadings to enhance the maximum power, analyze the output characteristics and compare the

TABLE 1. Comparison table summarizes the common and the similarities between the proposed and the previous related works.

Proposed work	To simulate the power output	48W Thin-Film Semitransparent (CdTe)-type and normal silicon-based modules, high transparency 40%	3 input neurons, 4 hidden neurons in a single layer and one output neuron	The mathematical expression of the power output	Compare with different equivalent modules	Accurate
[22]	To simulate the power output	210W semi-transparent Poly-crystalline Silicon, low transparency, about 10% average.	A simple model is created to simulate the power output using PV module thermal model	The mathematical expression of the power output	No	4.7% RMSE
[23]	To simulate the power output	semi-transparent c-Si glass-glass (G-G)i.e.	No	No	No	Accurate
[24], [25]	To simulate the power output	mono-crystalline (mono-), multi-crystalline (multi-), and amorphous (armor-) crystalline	2 input neurons, 3, 6, and 9 hidden neurons in a single layer and 2 output neuron	No	Yes	Accurate
[26]	To simulate the power output	BP150SX photovoltaic module	Not mentioned	No	No	Accurate
[27]	To simulate the power output	16 ITALSOLAR modules crystal silicon cells. 720W	2 input neurons, 7, and 9 hidden neurons in 2 layers and 2 output neuron	No	No	Accurate
[28]	To simulate PV temperature	92 kW BIPV system at PTM building.	5 input neurons, 4, and 3 hidden neurons in 2 layers and 1 output neuron	No	No	Accurate
[29]	To simulate the power output	900 watts capacity array	Not mentioned	No	No	Accurate

performance evaluation of these topologies under normal shading conditions. These analyses will provide an opportunity to select the best PV array topology in designing grid-connected and stand-alone PV systems.

A wireless, simple, low-cost monitoring system is also employed for a 6 × 50Wp laboratory scale STPV Module. The temperature, irradiance, voltage, and current of the array are acquired, processed and then transmitted to review the performance of the generation side. The acquired data are transmitted by a wireless method using an RF XBee signal (IEEE 802.15.4 standard) to control the acquisition system process without an extra microcontroller, unlike conventional systems. A MATLAB application program is built to graphically display the acquired data.

The remainder of this paper is organized into four sections. The first section presents a general review of the utilization of ANN to model the PV module. The second section briefly describes the procedure conducted to obtain the data points experimentally. The third section describes how the PV solar is modeled using experimental test data via the custom neural network coding from MATLAB®. The fourth section presents the results and discussions regarding the new formula of the Thin-Film PV system.

II. MODELING CONCEPT

Generally, the parameters of the equivalent circuit of a PV module primarily depend on the temperature and solar irradiance as well as the load variation, which is represented by the current. The dependence of the circuit parameters on environmental factors is investigated by using a set of current-voltage curves. The relationship between them is nonlinear and cannot be easily expressed by an analytical equation. Therefore, a neural network is utilized to overcome these difficulties [32]. The number of electronic applications using ANN-based solutions has increased considerably in the last few years. However, applications in PV systems have been very limited [27], [33].

In order to model a Thin-Film STPV performance and formulate its power output pattern, CNN-based modeling has been adopted. Surface temperature, solar irradiance, the load current, and the related power output are parameters concern the Thin-Film STPV that this work addresses for modeling and mathematically represents them.

III. CNN AND ITS LEARNING SCHEME

CNN is just a customized configuration of ANN, this work proposes CNN-based modeling as an algorithm to control the solutions of the ANN mathematical formulas and its network elements. With CNN, the selection of a number of neurons and their activation functions in the hidden layer is possible, which determines the number of the multivariable algebraic equations. The complexity of solving those equations reflect the computation time required to extract the power pattern equation of the PV system. Therefore, customize the network to achieve the goal of getting the power output modeling equation is the underlying cause to use CNN topology. It is a supervised ANN with a back-propagation learning rule (FIGURE 2.). This type of ANN is excellent at prediction tasks.

A single-layer perceptron is developed in terms of structure, weights, and learning process for the proposed modeling. The network weights are tuned via the learning process in which the network is trained. This algorithm iteratively continues for updating the weights until a specific condition is verified, which in this application stops when the error between the desired and the calculated CNN outputs reaches a predefined small value. The error is updated by optimizing

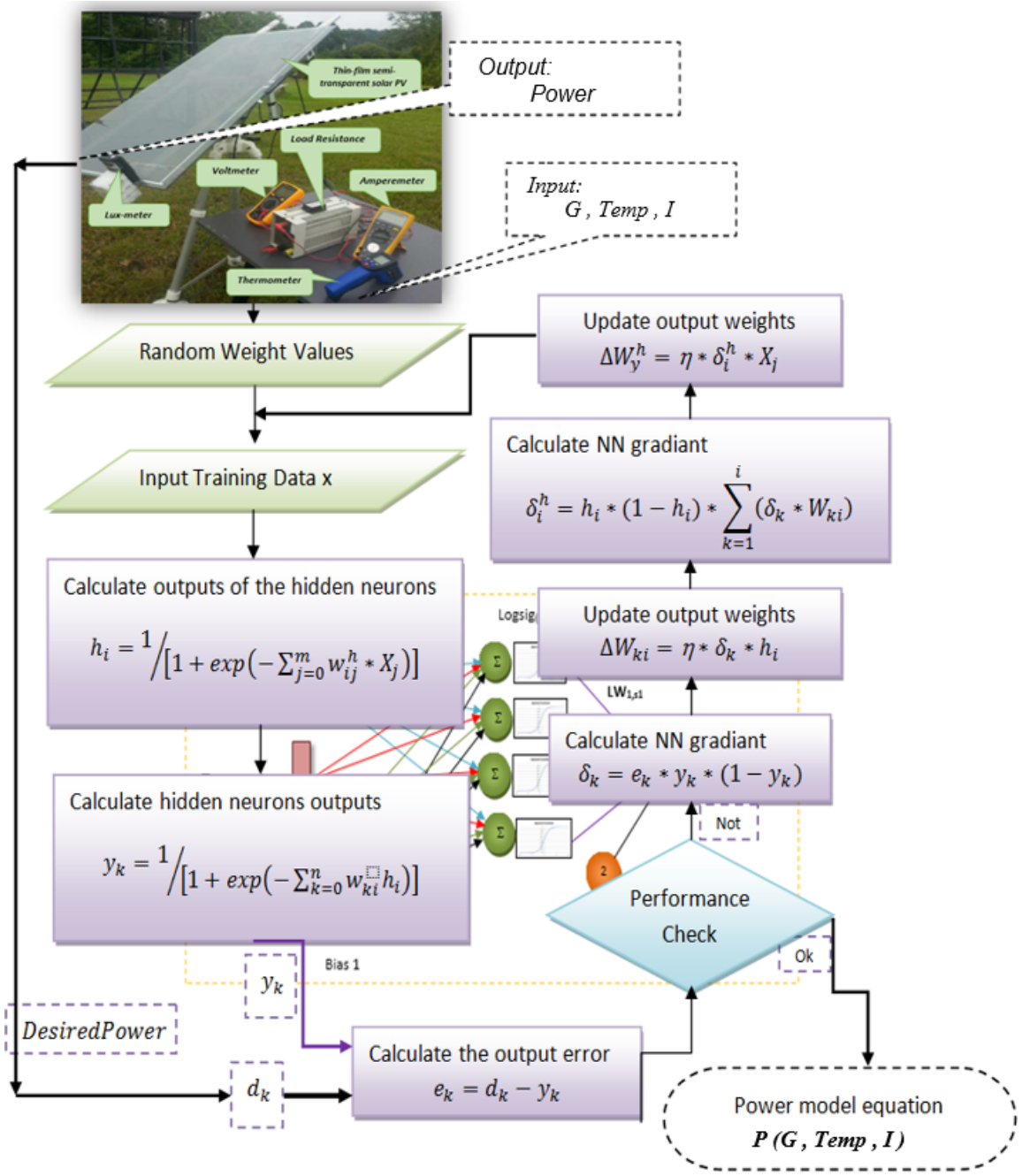

FIGURE 2. Modeling procedure diagram and CNN training algorithm for extracting the power model equation.

the weights and biases. After that, the developed CNN can be used to predict the power output as a function of the input parameters.

When the CNN generates the required output which means that it is trained to a satisfactory level, all the links between the units are stored. Those links or the weights are later used as an analytical expression tool to predict power output (P) for new input data set of irradiance (G), Temperature (Temp), and load current (I). Thus, the network model equation can be written as P = f(G, Temp, I). The associated training algorithm is presented in Algorithm 1.

A Thin-Film module with dimensions of (1200 × 600) mm, 48W peak power, and transparency of 40% is examined in this work. The modeling concept in a flowchart form of the proposed algorithm is shown in FIGURE 2.

IV. MATHEMATICAL MODELING-BASED CNN

Significant growth has been made in neural network knowledge, thus enlarging the range of potential applications in different areas due to the black box functionality of the neural network. ANN can offer very good mapping if taught properly [37]. The ANN structure is a significant factor in

Algorithm 1 Training Algorithm of the Proposed CNN

Input: Training set, irradiance dataset (G11)
temperature dataset (T11), Load Current (Current), Power
Input ← [G11;T11;Current]; %
Target ← Power;
Process: set a customized Feed forward net
Net ← newff(minmax(input),[4
1],{'logsig','purelin'},'trainlm');
net.trainparam.epochs ← 10000;
net.trainparam.goal ← 1e-25;
net.trainparam.lr ← 0.001;
net.trainparam.min_grad ← 8e-06;
[net,tr] ← train(net,input,Target);

Output: plotting the performance of the network and after the network has been trained, verify the input data set with the trained network by simulating the input dataset
plotperf(tr)
figure, Y ← sim(net,input); % P is some input data
plot(Y,'r-.','LineWidth',2)
hold on
plot(Target,'b-','LineWidth',2)
hold off
%% Viewing and extracting the weights of the network
view(net)
Iw ← cell2mat(net.IW);
b1 ← cell2mat(net.b(1))
Lw ← cell2mat(net.Lw)
b2 ← cell2mat(net.b(2))
Verification: testing the network by computing the network outputs
output ← net(Current);
%errors and overall performance.
errors ← gsubtract(Target,output);
performance ← perform(net,Target,output)
Saving the network parameters: saving the network parameters and results
netA31=net;
save netA31

manipulating the learning performance of networks, and the aim should be to utilize as small in structure as possible that meets the performance necessities under the environment. Experience has shown that using the minimum network that is able to learn the task is better for both theoretical and practical reasons.

Referring to Fig. 3, the input of the ANN module is represented by three components: irradiance, temperature, and the current as an expression for the load variation. The training set is used to adjust the weights during training. The testing or validation set is used to decide when to stop training. The root means square value (R) on the training set increases with successive training iterations, similar to the R on the test sets, up to a given point to avoid overtraining.

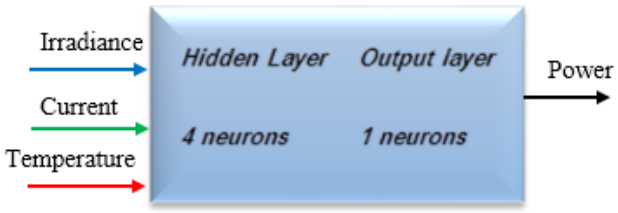

FIGURE 3. Configurations of the proposed ANN Model.

In this work, the Log-Sigmoid function is the activation formula that is used for the four hidden layer neurons, whereas a linear function is used in the output layer neuron, as in Fig. 4. The pure linear activation function is employed for the output layer to reduce the resulting computations.

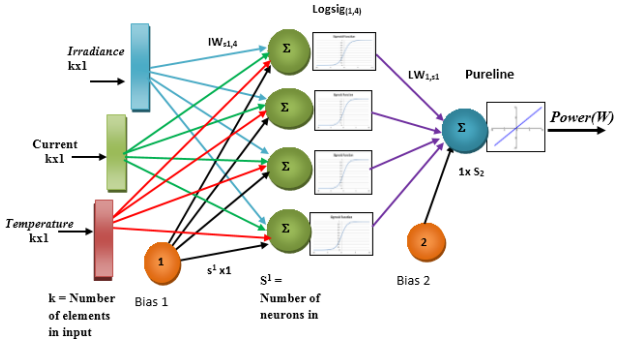

FIGURE 4. ANN PV module model.

To obtain the power output of the proposed network, the input layer is configured as a vector in three-dimensional space which includes three columns; irradiance G_k, temperature T_k, and current I_k. The data samples are represented by the index (k): where $k = (k_1, k_2, k_3 \ldots k_R)$. Thus, the input vector components are G_k, T_k, and I_k, while the hidden layer, which has four neurons can be written as $n^1_{1,4}$. The output of the neurons in the hidden layer given by $A^1_{1\_4}$. Thus:

$$f_1(n) = logsig(n), \quad logsig\left(A^1_4\right) = \frac{1}{1 + e^{-n^1_{1\_4}}}$$

where

$$n^1_1 = G * Iw_{(1,1)} + T * Iw_{(1,2)} + I * Iw_{(1,3)} + b^1_{(1,1)} \quad (1)$$

$$A_1 = {}^1\Big/\left(1 + e^{(-n^1_1)}\right) \quad (2)$$

$$n^1_2 = G * Iw_{(2,1)} + T * Iw_{(2,2)} + I * Iw_{(2,3)} + b^1_{(2,1)} \quad (3)$$

$$A_2 = {}^1\Big/\left(1 + e^{(-n^1_2)}\right) \quad (4)$$

$$n^1_3 = G * Iw_{(3,1)} + T * Iw_{(3,2)} + I * Iw_{(3,3)} + b^1_{(3,1)} \quad (5)$$

$$A_3 = {}^1\Big/\left(1 + e^{(-n^1_3)}\right) \quad (6)$$

$$n^1_4 = G * Iw_{(4,1)} + T * Iw_{(4,2)} + I * Iw_{(4,3)} + b^1_{(4,1)} \quad (7)$$

$$A_4 = {}^1\Big/\left(1 + e^{(-n^1_4)}\right) \quad (8)$$

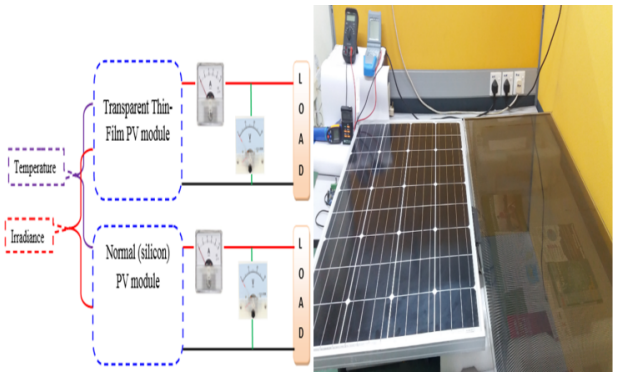

FIGURE 5. Laboratory experimental setup to extract the P-V characteristic curves between two equivalent PVs (STPV & silicon-based PV) by measuring 4 parameters.

The net input to the neurons in the output layer, which has one layer $A^2_{1\_1}$, is given by:

$$A^2_{1\_1} = f_2\left(n^2_1\right) = pureline\left(n^2_1\right) = 1$$

The output of the neural network $\text{ANN}_{\text{output}}$ resulting from data training is given by Eq. (9):

$$ANN_{output} = A_1 * Lw_{(1,1)} + A_2 * Lw_{(1,2)} + A_3 * Lw_{(1,3)} + A_4 * Lw_{(1,3)} + A^2_{1\_1} * b^2_{(1,1)} \quad (9)$$

Iw, *Lw*, b^1, b^2 are the weight matrices of the associated input, hidden and bias layers, respectively. The solving of four symbolic equations are described in Algorithm 2.

V. EXPERIMENTAL SETUP

The power output of PV modules can be predicted from the behavior of the current-voltage, I-V, and power-voltage, P-V, characteristic curves [34]. The P-V characteristic curve of a PV panel at standard conditions (1000 W/m^2 irradiation and ambient temperature, 25°C) is provided with the manufacturer specification sheet. Therefore, the P-V characteristic curves at conditions other than standard can be measured experimentally by connecting the PV module to a high-power, variable resistor representing the load and continuously measuring both the voltage and current for each individual step of the module surface temperature and irradiance.

Thin-Film modules with the same dimensions (1200 × 600) mm, but different power values of 48W, 64W, and 72W with their associated transparencies of 40%, 20%, and 10%, respectively, are examined. Two types of experimental measurements are implemented: laboratory- and field-based experiments.

A. LAB-BASED EXPERIMENTAL SETUP

Since the study objective is to highlight the power output and the module behavior under a variety of weather conditions, the measurements of the STPV are presented by comparing each P-V curve under a constant irradiance/temperature pair with its equivalent silicon-based PV module.

Algorithm 2 Solving of Four Symbolic Equations of the Proposed CNN

Input: Reload the network parameters, that have the name (netA31)
load netA31
Process: Solving the symbolic equations
I ← Current;
G ← G11;
T ← T11;
Defining: Syms ← G, T, I
% 1st hidden neuron equations
N1 ← G*Iw(1,1) + T*Iw(1,2)+I*Iw(1,3)+b1(1,1)
A1 ← 1 / (1+exp (− N1))
N2 ← G*Iw(2,1)+T*Iw(2,2)+I*Iw(2,3)+b1(2,1)
A2 ← 1 / (1+exp (− N2))
N3 ← G*Iw(3,1)+T*Iw(3,2)+I*Iw(3,3)+b1(3,1)
A3 ← 1 / (1+exp (− N3))
N4 ← G*Iw(4,1) + T*Iw(4,2)+I*Iw(4,3)+b1(4,1)
A4 ← 1 / (1+exp (− N4))
% calculate the network output power
Powers ← vpa(Lw(1,1)*A1+Lw(1,2)*A2+Lw(1,3)*A3+Lw(1,4)*A4+b2(1,1))
% simplify and substitute the variables
powG ← subs(powers,G,500);
powT ← subs(powG,T,20);
powers ← subs(powT,I,0.2949);
Output: The simplified power output
R ← vpa(powerss)

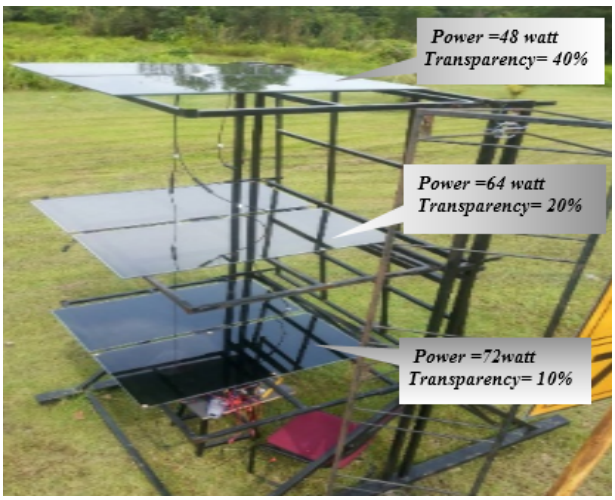

FIGURE 6. Multilayer setup for semitransparent Thin-Film PV.

The lab experimental tests were conducted on Thin-Film type PV CdTe with 48W/40% transparency. An irradiance range of 0-1000 W/m2 was applied to two values of module temperature (30 and 45 °C). For comparison, the same conditions were applied on an equivalent silicon-based blind PV module with the same power and open circuit voltage Voc. The experimental setup can be described by the diagram in Fig. 5.

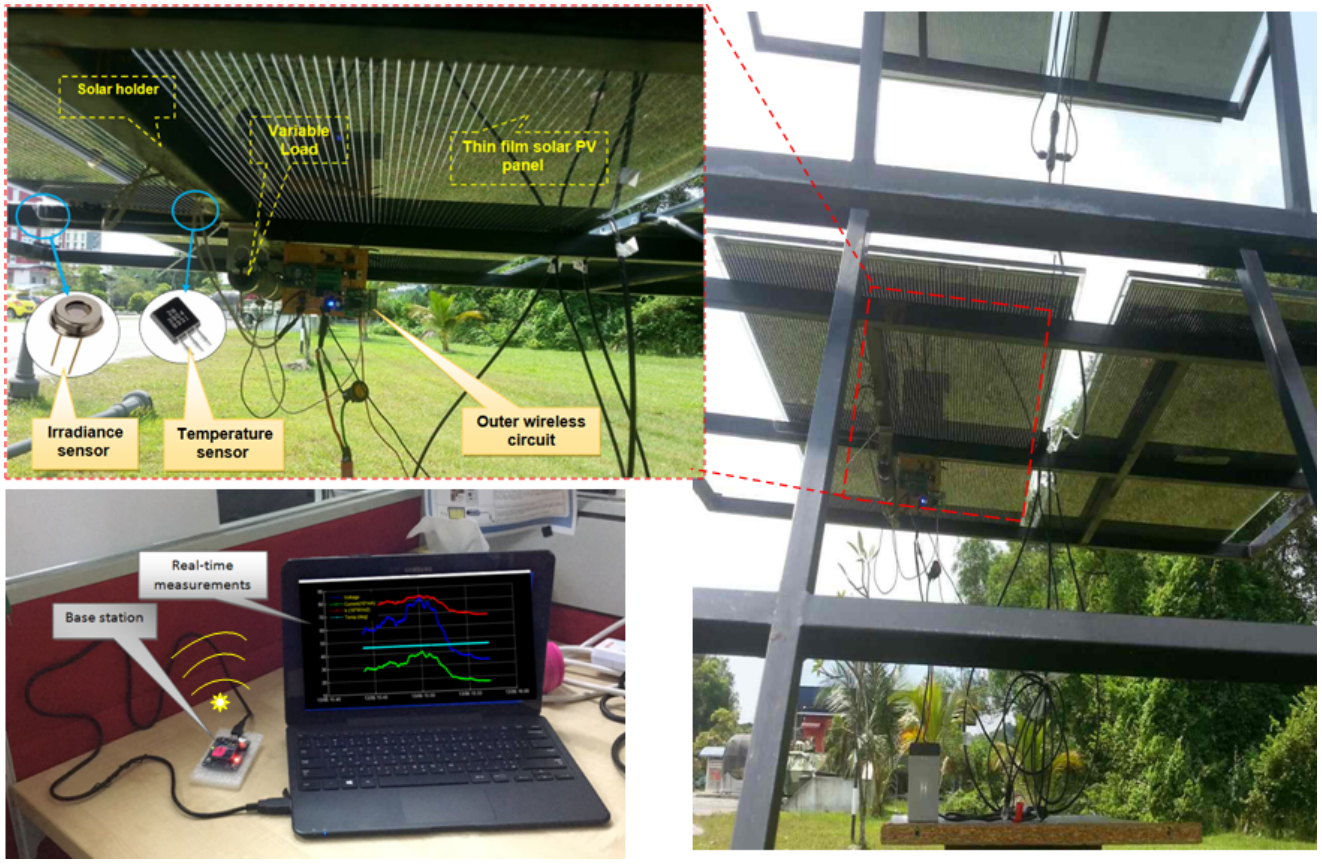

FIGURE 7. A monitoring system for the experimental measurements for the Thin-Film PV.

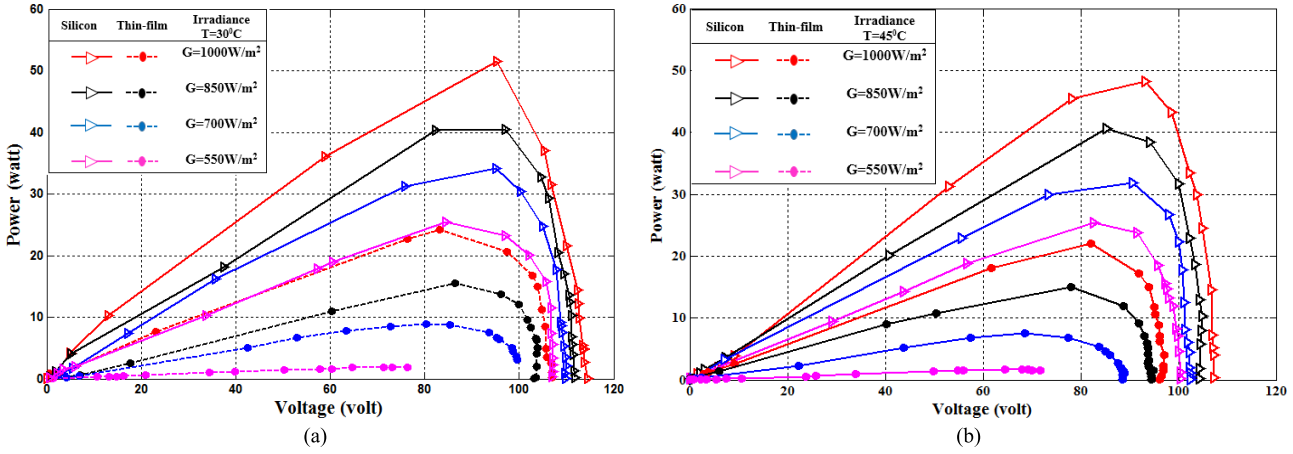

FIGURE 8. P-V curves of the lab experimental measurements for two equivalent modules, (a) STPV and (b) Silicon-based PV, under various irradiation values at temperatures of 30 °C (a) and 45 °C (b).

B. FIELD-BASED EXPERIMENTAL SETUP

A multilayer installation category was conducted for analysis, and the attained data were processed individually. To facilitate the gathering of information from the panels, a wireless RF remote node represented by the XBee module was utilized. XBee modules were chosen because they are easy to work with and have demonstrated adequate performance in different types of applications [35], [36]. A monitoring center attached to central computer stores and displays relevant data from the PV panel. The monitoring center is aware of the solar panel structure and thus can aggregate the acquired information from the remote node.

Three layers configuration of Thin-Film STPV modules, started with the higher transparency modules from the top,

were connected in series for power analysis purposes. The setup of the experiment is shown in Fig. 6.

A low cost and low consumption wireless monitoring system, which is published in a previous effort [30], [31]. This hardware includes an ACS754 current sensor, which had a maximum current limit of 5 Amp and sensitivity of 3.8 mV/A, to measure the PV array, which had a maximum current of 3Amp. The circuit has only a couple of XBee RF modules as active components and other passive components, resistors, and capacitors, for measuring the PV current, voltage. The irradiance was measured by an (LDR) sensor placed in parallel with the panels, and a temperature sensor was placed in contact with the down surface of one panel from the array via LM35. A temperature sensor with a sensitivity of 10 mV/°C was used to measure the surface temperature of the solar panel. The system has four channels with the adjustable sampling frequency, up to 14 sample/sec in some application cases of short period data logging. For voltage acquisition, a 1kΩ voltage divider was used, corresponding to 10mV for every one volt of DC output. The remote node comprises single RF XBee module, which is configured to access the 4 analog signals, that mentioned above, for processing via the built-in ADC and transmitting the data wirelessly to a base station node, which in turn was linked directly to a PC. The experimental setup for monitoring the PV data is shown in Fig. 7.

Measurements of both the electrical (voltage and current) and environmental (irradiance and temperature) values were received by the base/central node via an IEEE 802.15.4 low-rate wireless standard.

VI. RESULTS AND DISCUSSION

A. SINGLE-PANEL ANALYSIS

1) LAB-BASED EXPERIMENTAL RESULTS

Fig. 8 (a and b) shows the P-V curves for the lab experimental measurements for two equivalent modules, STPV, and Silicon-based PV, under various irradiation values at temperatures of 30 °C (a) and 45 °C (b).

A significant difference is clear between the two equivalent tested modules, which indicates the threshold value at which the STPV starts generating power. The analysis shows similar influences of the weather conditions (irradiance and temperature) on the power pattern. For example, the maximum power point at 1000W/m2 and 45oC for the STPV is approximately 22W, in contrast, a value of approximately 48W is measured for the equivalent silicon-based PV, as indicated in Fig. 8 (b).

As in the silicon-based PV behavior, Fig. 8 shows the dependence of the module current and voltage on irradiance and temperature. Irradiance affects the module current; the higher the irradiance, the higher the current drawn by the PV module. The temperature affects the module voltage; the higher the temperature, the lower the voltage on the module terminal. Both figures show the point where the product of the PV array voltage and current reaches the maximum value, i.e., the maximum power point (MPP), in which the PV module operates with maximum efficiency and produces maximum output power. The variation of the irradiance and temperature in the PV module is characterized as a short time fluctuation that follows the behavior of atmospheric conditions around the module during that time. The effect of this variation is the unpredictable variation of the power output, current, and voltage of the module.

Fig. 8 also shows that the voltage Voc changes slightly with irradiation. The values of Isc and Voc with solar irradiance are similar to those for the different types of Thin-Film PV panels. The surface temperature of the panel has a significant effect on Voc, which decreases as the temperature increases. Therefore, thermal equilibrium of PV surface must be achieved during the P-V test for the results to be accurate.

The most significant behavior that can be clearly observed is that this type of PV begins electrical generation at a level higher than 500W/m^2. However, the other characteristics tend to be similar to those of the equivalent silicon-based PV, as will be demonstrated in the field-measurement experimental test.

The temperature decreases linearly with the output voltage, in contrast to the current. As a result, the reduction of the voltage lowers the power output of the PV panel at constant solar irradiation. The effect of temperature on the short circuit current is small but increases with increasing irradiance.

2) FIELD-BASED EXPERIMENTAL RESULTS

Referring to Fig. 7, the measurement and gathering processes are conducted by the sensor remote node with a configurable sample time. The configuration of the proposed solution is highly flexible and depends on the number of PV modules, strings, arrays, and the layout of the PV installation. A comparison-based measurement was conducted to discover the behavior of the Thin-Film STPV module. The measurements started at approximately 7:00 am and ended at 7:00 pm. The same power was used for both (48W) PV modules, which were tested under the same weather conditions, as shown in Fig. 9.

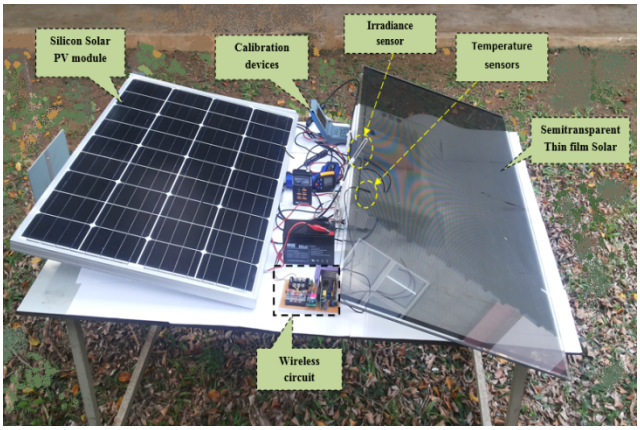

FIGURE 9. Field-based experimental measurements for one Thin-Film STPV and its equivalent silicon-based modules.

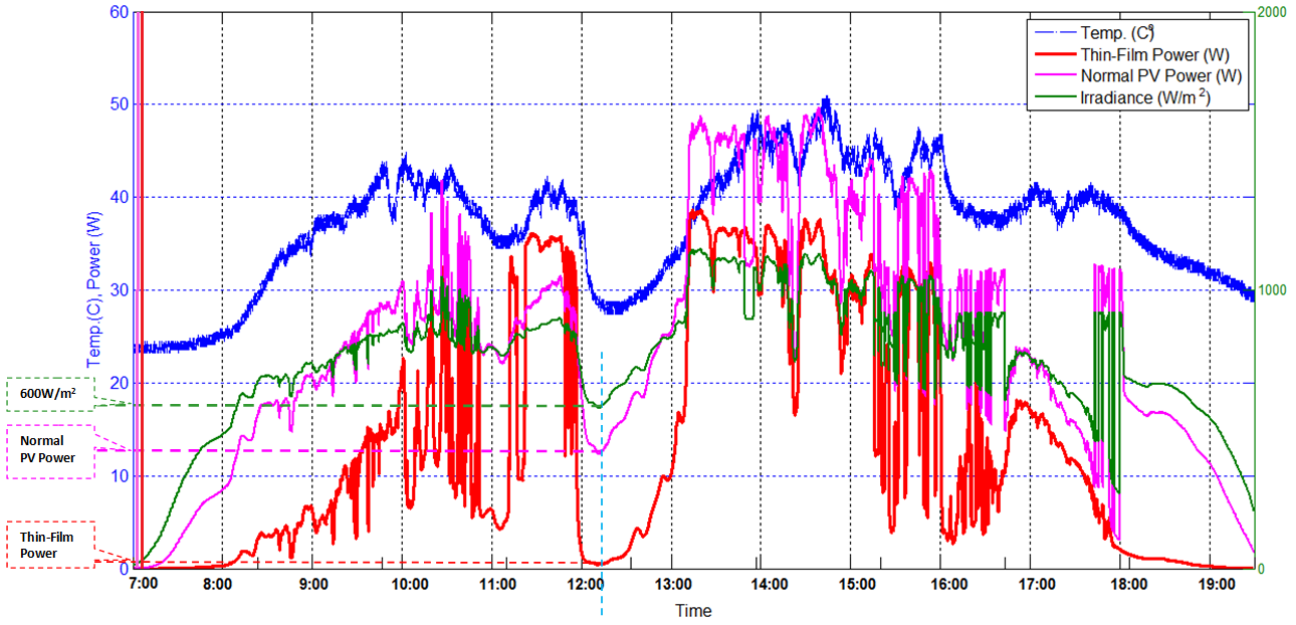

FIGURE 10. The daily measurements of 3 parameters and comparison with the equivalent silicon module on 4/7/2017.

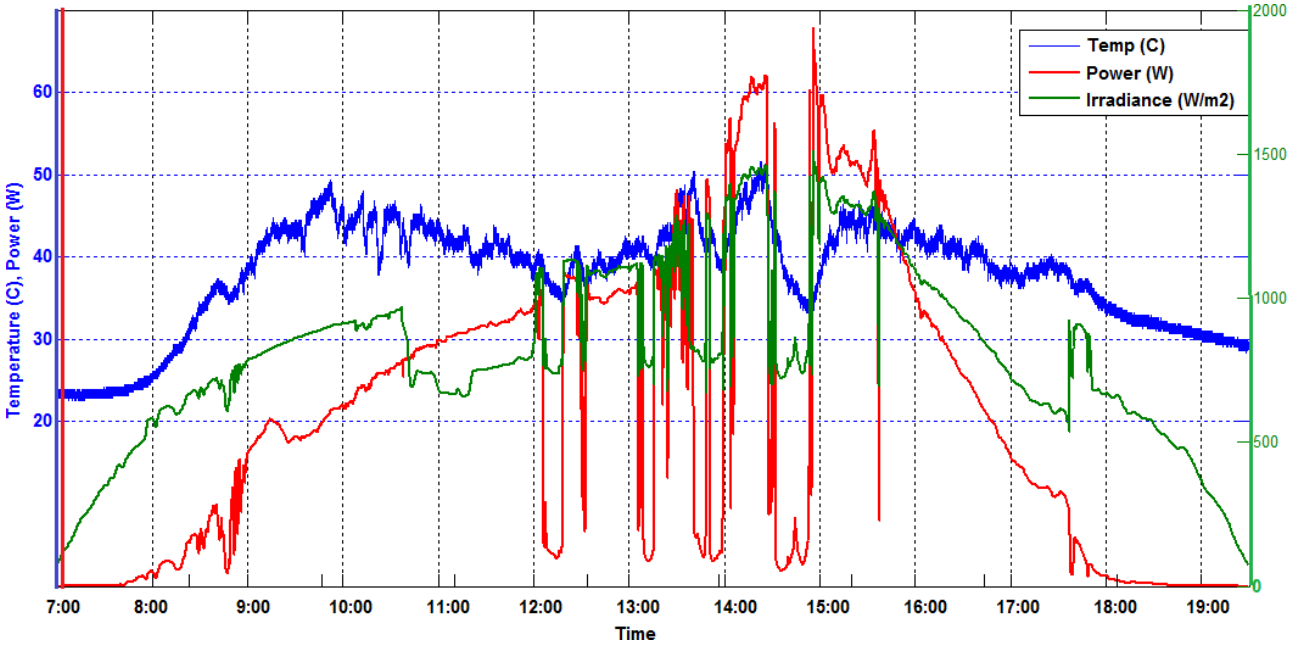

FIGURE 11. The daily measurements of three parameters for the multilayer configuration on 2/7/2017.

Cloudy day measurements were selected to present the data showing the effect of shading on both modules. To compare their behaviors, the two weather parameters with the generated power for the Thin-Film and silicon modules are shown in Fig. 10.

Although the power patterns of both tested PV modules were relatively similar, the results showed a significant difference in output power between the two modules. The silicon-based module can generate power starting at very low irradiance levels, whereas the Thin-Film STPV module starts generation at approximately 600 W/m^2. This drawback limits the generated power for the Thin-Film STPV to a certain level of irradiance compared to the blind PV.

B. MULTILAYER ANALYSIS

Referring to Fig. 6, and to study the effect of shading and multilayer installation of the STPV system, a series of 6 connected PV modules was used. The top layer included

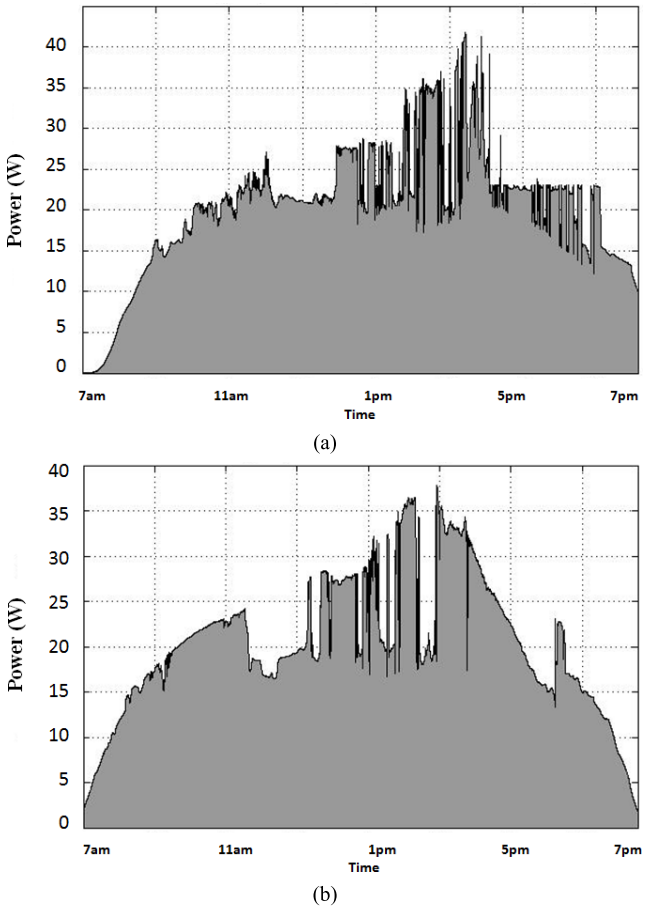

FIGURE 12. Harvested energy on 5 July 2018: (a) for a single module and (b) for a multilayer module.

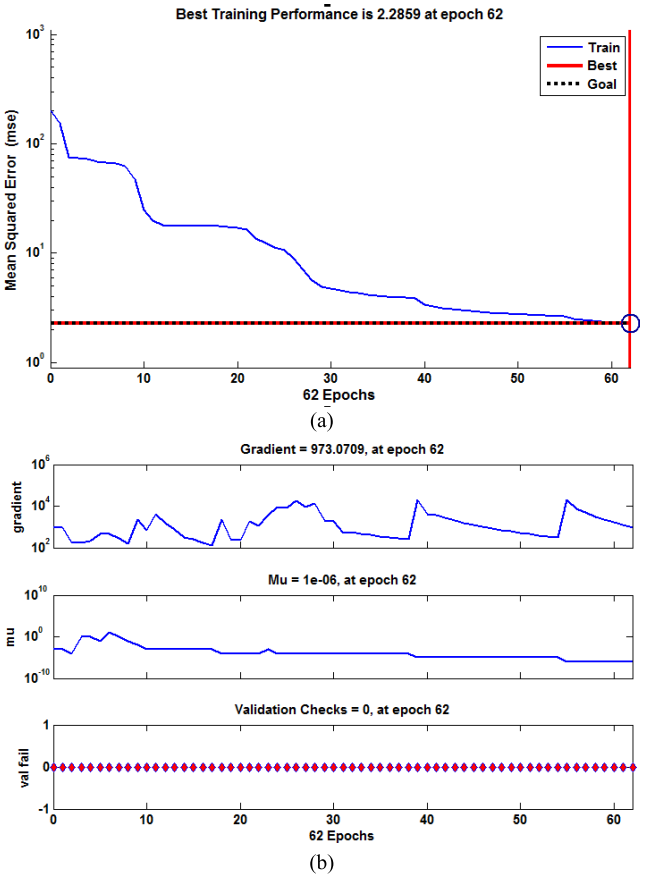

FIGURE 13. The proposed CNN (a) Training performance, (b) Training state.

two modules with 48W and 40% transparency, the middle layer contained a second pair with 62W and 20% transparency, and the bottom layer included a pair of modules with 72W and 10% transparency. One sample of daily measurements of three parameters for the multilayer configuration on 2/7/2017 is shown in Fig 11.

The solar power output was calculated according to Ohm's law given by equation (10):

$$Power_{out}\,(W) = V * I \tag{10}$$

The quantity of energy E_out (Wh), which represents the area under the power rate curve, is given by Eq. (11):

$$E_{out}(Wh) = \int_{7am}^{7pm} P\,(t)\,dt \tag{11}$$

The harvested (Wh) energy attained from single and multilayer configurations are calculated either by using the above integration formula or numerically by applying the trapezoidal method. Therefore, for simplicity, a MATLAB function is utilized to obtain the area under the power rate curve based on the results of the trapezoidal integration method. Using this monitoring system to collect the energy data, the results for 5 July 2018 for the single and multilayer installation are presented in Fig. 12 (a and b).

The daily harvested energy is 190.01Wh for a single module and 218.48Wh for the multilayer configuration. These negative results indicate that there it is infeasible to employ this configuration at PV installation. Furthermore, since each individual Thin-Film module can only generate power at a specific high level of irradiance, natural shading or that due to the multilayer will block the energy generation. Therefore, in this study, the modeling concept considers only the single-layer configuration which is represented by one module.

C. NEURAL NETWORK TRAINING RESULTS

The maximal sum of epochs was fixed at 1000, which is the default number. Accordingly, the training scale was also fixed to the default number and allowed to modify accordingly as the training process increased. The relationship between the developed CNN model and the measured data harvested experimentally can be expressed with the correlation coefficient as shown in Fig. 13 (a) and (b), where the best validation performance is 2.2859 at epoch 62.

To evaluate the network performance, the correlation coefficient (R2) is adopted according to the equation given in (12):

$$R^2 = 1 - \left[\frac{\sum_{k=1}^{k_R}(f(x_K) - y_K)^2}{\sum_{k=1}^{k_R}(f(x_K) - [\frac{1}{K_R}\sum_{k}^{K_R} f(x_k)])^2}\right] \tag{12}$$

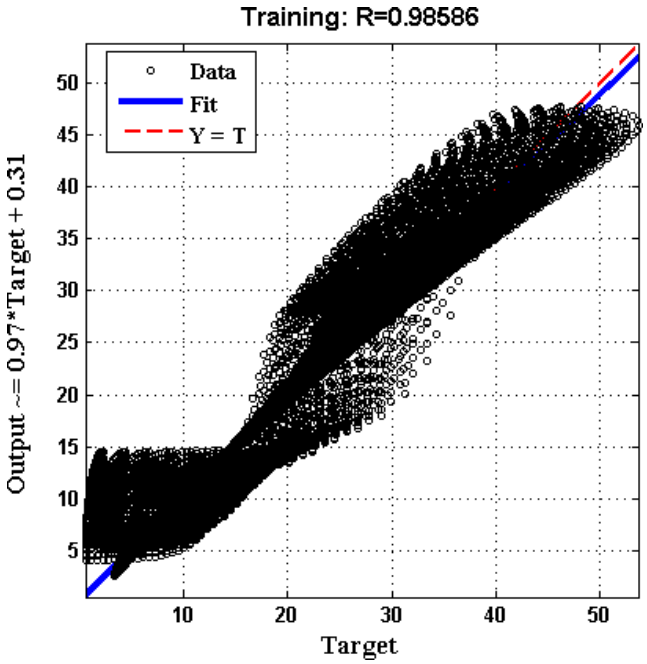

FIGURE 14. The correlation coefficient results for CNN training.

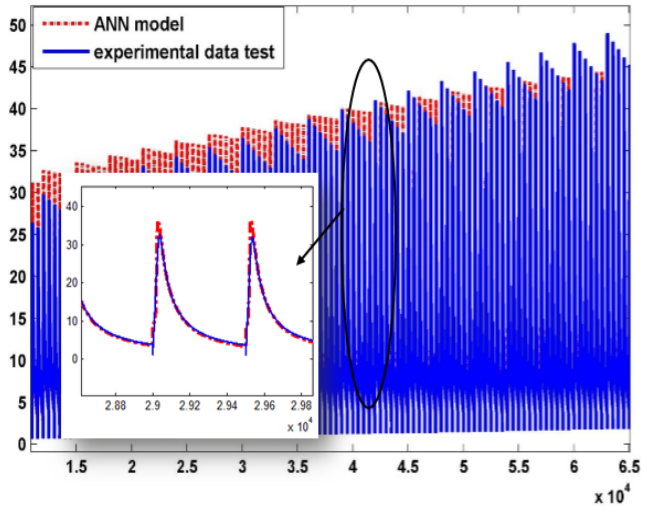

FIGURE 15. The comparison curves under a wide range of input data.

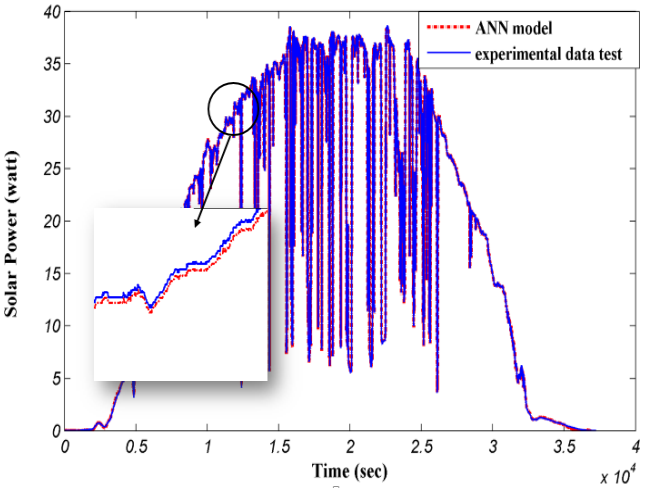

FIGURE 16. Comparison of daily measurements and the developed CNN model for Thin-Film STPV.

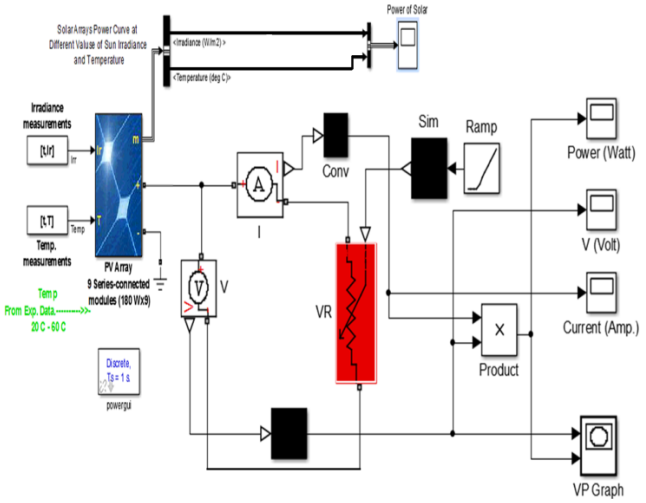

FIGURE 17. Simulation diagram of the two diode-based PV model with experimental input data set for comparison purpose with CNN-based PV.

where K_R denotes the data points that are required to calculate the sum of squares and x_K and y_K refer to the experimental and simulated data, respectively.

Because the value of the correlation coefficient has a relatively excellent value as it approaches unity, we can simulate a wide range of input data for the proposed model as values of irradiance G, temperature T and current I. To create the neural network model, a series of input data were used, including vectors of irradiance (G), temperature (T) and current (I), on which the neural network was based to train the weights. The number of hidden neurons specifies the complexity of the generated mathematical formula. The four neurons in the hidden layer are fully connected to the inputs and participate in the estimated output. Sigmoid activation functions are used for the hidden neurons, while a pure linear activation function is used for the output neuron.

The results show a significant convergence between the experimental and CNN outcomes, as is clearly evident in the correlation coefficient in Fig. 14 and the comparison curves under a wide range of input data shown in Fig. 15.

After substituting, solving, and simplifying the network symbolic equations, the formula corresponding to the mathematical model that is generated by the neural network can be given in Eq. (13):

$$Power = \frac{3.1746}{\left(2990039237.2 * e^{6.37\mathbf{G}} * e^{0.05*\mathbf{T}} * e^{-7.6264\mathbf{I}} + 0.1\right)} - \frac{11.12268}{\left(39.51557 * e^{2.579*\mathbf{T}} * e^{12.962\mathbf{I}} + 0.1\right)} - \frac{5051.904}{\left(344.26 * e^{1.012\mathbf{G}} * e^{-1717.263*\mathbf{I}} + 0.1\right)} - \frac{150.811}{\left(1.3667 * e^{3.092*\mathbf{I}} + 0.1\right)} + 63.2961 \quad (13)$$

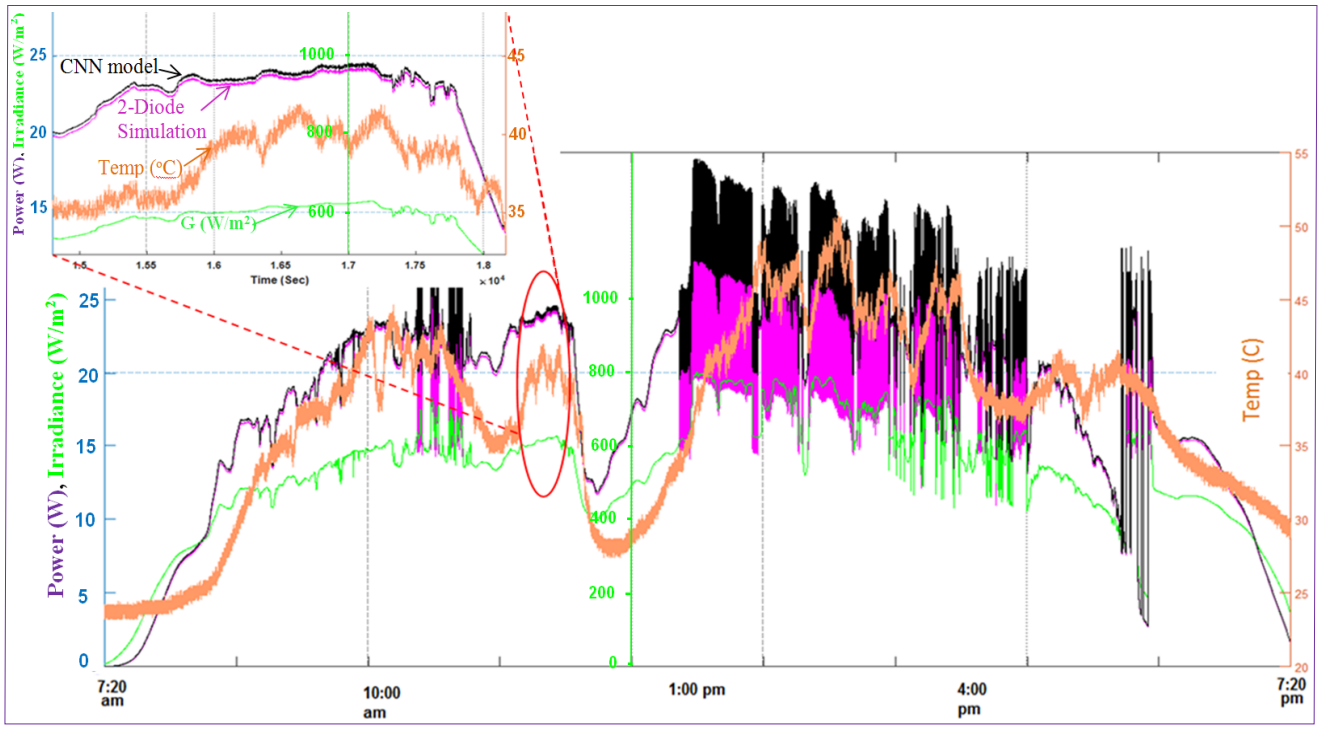

FIGURE 18. Comparison between the power output of the two- diode MATLAB Simulation and the proposed CNN models with the variation of irradiance, and Panel temperature along with time on a normal day.

Since the sampling frequency was approximately one sample per second, the input matrix dimension was (43200, 3) for logging 12 hours of data. Each row of input data was simply composed of (solar radiation and ambient temperature, current) for use during the training process of the CNN. The obtained correlation coefficient was 0.986. Thus, once the proposed CNN has been trained, it can estimate the module power outcome even for the data that is not used during the training process with acceptable accuracy.

Fig. 16 shows a comparison of a full daytime logging of Thin-Film data between the measurements and the CNN model power. There is obviously a good fit between the measured data and modeled data.

Additional training experimental data for a different day were processed to present another power pattern of the PV module with the power formula given by Eq. (14):

$$Power = \frac{19.7307}{(exp\,(10.6576 * G - 9.44 * I + 5.74 * T - 2.202) + 1.0)} - \frac{79.6}{(exp\,(0.032 * G + 0.035 * T - 3.429) + 1.0)} + 76.514 \quad (14)$$

The smaller sampling time improves the accuracy of modeling and captures the potential surge of power.

D. CNN MODEL EVALUATION

Since there is no equivalent model for STPV module to compare, the performance evaluation for the proposed CNN-based PV system is performed via comparing its effectiveness on the silicon-based PV with the two-diode model PV in the MATLAB-based simulation. The same experimental data set for the irradiance and the temperature have been applied to both models. The simulation diagram is shown in Fig.17.

Those weather parameters were varying along with the daytime at about 1 sample/sec. The two power output for both simulation-based and CNN-based models are displayed with variations of the panel temperature and irradiance are shown in Fig. 18.

It is clear that the power output of proposed CNN-based model verified that of the simulation outcome, which proves the success of the developed CNN as modeling expression for STPV system, and the possibility to implement CNN-model PV system in real-life applications to enhance PV energy extraction, and the power quality for the modeling of PV power systems.

VII. CONCLUSIONS

This work developed a CNN as a customized ANN to formulate the power output pattern of a Thin-Film STPV module. The accuracy and generalization of the proposed model were validated by comparing measurements with a proposed CNN module on different logging days. The most significant contributions are the following: (a) a limit at which this type of PV can start generating power is assigned; (b) based on CNN modeling, a mathematical expression is provided for the power profile that depends only on the experimentally measured parameters and can be used as a reference

supporting the manufacturer datasheet; (c) the P-V and I-V curves of the STPV module are similar in shape but not values to those of a silicon-based solar module; (d) since each individual Thin-Film module can only generate power at a specific high level of irradiance, natural shading or that due to the multilayer will block energy generation.

REFERENCES

[1] F. Zaoui, A. Titaouine, M. Becherif, M. Emziane, and A. Aboubou, "A combined experimental and simulation study on the effects of irradiance and temperature on photovoltaic modules," *Energy Procedia*, vol. 75, pp. 373–380, Aug. 2015.
[2] I. M. Dharmadasa *et al.*, "Fabrication of CdS/CdTe-based thin film solar cells using an electrochemical technique," *Coatings*, vol. 4, no. 3, pp. 380–415, 2014.
[3] A. Ibrahim, "Analysis of electrical characteristics of photovoltaic single crystal silicon solar cells at outdoor measurements," *Smart Grid Renew. Energy*, vol. 2, no. 2, pp. 169–175, 2011.
[4] A. Yano, M. Onoe, and J. Nakata, "Prototype semi-transparent photovoltaic modules for greenhouse roof applications," *Biosyst. Eng.*, vol. 122, pp. 62–73, Jun. 2014.
[5] C. J. M. Emmott *et al.*, "Organic photovoltaic greenhouses: A unique application for semi-transparent PV?" *Energy Environ. Sci.*, vol. 8, no. 4, pp. 1317–1328, 2015.
[6] *Transparent Solar Panels Semi Transparent Solar Panels*. Accessed: Mar. 3, 2018. [Online]. Available: http://www.solar-constructions.com/wordpress/transparent-solar-panels/
[7] A. Chatterjee, A. Keyhani, and D. Kapoor, "Identification of photovoltaic source models," *IEEE Trans. Energy Convers.*, vol. 26, no. 3, pp. 883–889, Sep. 2011.
[8] A. Chouder, S. Silvestre, N. Sadaoui, and L. Rahmani, "Modeling and simulation of a grid connected PV system based on the evaluation of main PV module parameters," *Simul. Model. Pract. Theory*, vol. 20, no. 1, pp. 46–58, 2012.
[9] T. Ma, H. Yang, and L. Lu, "Solar photovoltaic system modeling and performance prediction," *Renew. Sustain. Energy Rev.*, vol. 36, pp. 304–315, Aug. 2014.
[10] S. Bal, A. Anurag, and B. C. Babu, "Comparative analysis of mathematical modeling of photo-voltaic (PV) array," in *Proc. Annu. IEEE India Conf.*, vol. 8, 2012, pp. 269–274.
[11] M. H. El-Ahmar, A. H. M. El-Sayed, and A. M. Hemeida, "Mathematical modeling of photovoltaic module and evalute the effect of varoius paramenters on its performance," in *Proc. 18th Int. Middle East Power Syst. Conf. (MEPCON)*, 2016, pp. 741–746.
[12] P. V. Bernhardt, G. K. Boschloo, F. Bozoglian, A. Hagfeldt, and M. Martínez, "Study of the equivalent circuit of a dye-sensitized solar cells," *Adv. Energy Int. J.*, vol. 1, pp. 1–2, 2014.
[13] H. Patel and V. Agarwal, "MATLAB-based modeling to study the effects of partial shading on PV array characteristics," *IEEE Trans. Energy Convers.*, vol. 23, no. 1, pp. 302–310, Mar. 2008.
[14] N. A. Zainal and A. R. Yusoff, "Modelling of photovoltaic module using MATLAB Simulink," in *Proc. IOP Conf. Ser., Mater. Sci. Eng.*, vol. 114, no. 1, 2016, p. 12137.
[15] A. H. Sabry, W. Z. W. Hasan, M. Z. A. A. Kadir, M. A. M. Radzi, and S. Shafie, "Field data-based mathematical modeling by Bode equations and vector fitting algorithm for renewable energy applications," *PLoS ONE*, vol. 13, no. 1, p. e0191478, Jan. 2018.
[16] T. Khatib, A. Mohamed, K. Sopian, and M. Mahmoud, "Assessment of artificial neural networks for hourly solar radiation prediction," *Int. J. Photoenergy*, vol. 2012, Feb. 2012, Art. no. 946890.
[17] A. Saberian, H. Hizam, M. A. M. Radzi, M. Z. A. A. Kadir, and M. Mirzaei, "Modelling and prediction of photovoltaic power output using artificial neural networks," *Int. J. Photoenergy*, vol. 2014, Apr. 2014, Art. no. 469701.
[18] M. H. M. Sidek, N. Azis, W. Z. W. Hasan, M. Z. A. A. Kadir, S. Sha, and M. A. M. Radzi, "Automated positioning dual-axis solar tracking system with precision elevation and azimuth angle control," *Energy*, vol. 127, pp. 160–170, Apr. 2017.
[19] T. Verma, A. P. S. Tiwana, C. C. Reddy, V. Arora, and P. Devanand, "Data analysis to generate models based on neural network and regression for solar power generation forecasting," in *Proc. 7th Int. Conf. Intell. Syst., Modelling Simulation*, 2016, pp. 97–100.
[20] L. Sandrolini, M. Artioli, and U. Reggiani, "Numerical method for the extraction of photovoltaic module double-diode model parameters through cluster analysis," *Appl. Energy*, vol. 87, no. 2, pp. 442–451, Feb. 2010.
[21] F. Nakanishi, K. Ebihara, T. Ikegami, T. Maezono, and Y. Yamagata, "Estimation of equivalent circuit parameters of PV module and its application to optimal operation of PV system," *Sol. Energy Mater. Sol. Cells*, vol. 67, nos. 1–4, pp. 389–395, 2001.
[22] C. Y. Huang, H. J. Chen, C. C. Chan, C. P. Chou, and C. M. Chiang, "Thermal model based power-generated prediction by using meteorological data in BIPV system," *Energy Procedia*, vol. 12, pp. 531–537, Sep. 2011.
[23] R. Beniwal, G. N. Tiwari, and H. O. Gupta, "An algorithm to predict accurate output power of a glass-glass (semitransparent) solar thermal module using artificial neural network," *Int. J. Eng. Technol.*, vol. 9, no. 3, pp. 1542–1550, 2017.
[24] W. Xiao, G. Nazario, H. Wu, H. Zhang, and F. Cheng, "A neural network based computational model to predict the output power of different types of photovoltaic cells," *PLoS ONE*, vol. 12, no. 9, p. e0184561, 2017.
[25] V. L. Brano, G. Ciulla, and M. Di Falco, "Artificial neural networks to predict the power output of a PV panel," *Int. J. Photoenergy*, vol. 2014, Jan. 2014, Art. no. 193083.
[26] A. Guessoum, H. Mekki, A. Mellit, and H. Salhi, "Artificial neural network-based modeling and monitoring of photovoltaic generator," *Medit. J. Model. Simul.*, vol. 3, pp. 1–9, Jan. 2015.
[27] H. Mekki, A. Mellit, H. Salhi, and B. Khaled, "Modeling and simulation of photovoltaic panel based on artificial neural networks and VHDL-language," in *Proc. IEEE Int. Conf. Electron., Circuits, Syst.*, Dec. 2007, pp. 58–61.
[28] L. Yalcin and R. Ozturk, "Performance comparison of c-Si, mc-Si and a-Si thin film PV by PVsyst simulation," *J. Optoelectron. Adv. Mater.*, vol. 15, nos. 3–4, pp. 326–334, 2013.
[29] H. Parmar, "Artificial neural network based modelling of photovoltaic system," *Int. J. Latest Trends Eng. Technol. Artif.*, vol. 5, no. 1, pp. 3505–3513, 2015.
[30] A. H. Sabry, W. Z. W. Hasana, M. Z. A. A. Kadir, M. A. M. Radzi, and S. Shafie, "Low cost wireless sensor monitoring system for photovoltaic (PV) array parameters," in *Proc. IEEE 4th Int. Conf. Smart Instrum., Meas. Appl. (ICSIMA)*, Nov. 2017, pp. 1–6.
[31] A. H. Sabry, W. Z. W. Hasan, M. Z. A. A. Kadir, M. A. M. Radzi, and S. Shafie, "DC-based smart PV-powered home energy management system based on voltage matching and RF module," *PLoS ONE*, vol. 12, no. 9, pp. 1–22, 2017.
[32] E. Karatepe, M. Boztepe, and M. Colak, "Neural network based solar cell model," *Energy Convers. Manag.*, vol. 47, nos. 9–10, pp. 1159–1178, 2006.
[33] M. Hadjab, S. Berrah, and H. Abid, "Neural network for modeling solar panel," *Int. J. Energy*, vol. 6, no. 1, pp. 9–16, 2012.
[34] A. Q. Jakhrani, S. R. Samo, S. A. Kamboh, J. Labadin, and A. R. H. Rigit, "An improved mathematical model for computing power output of solar photovoltaic modules," *Int. J. Photoenergy*, vol. 2014, Mar. 2014, Art. no. 346704.
[35] M. A. Nasirudin, U. N. Za'bah, and O. Sidek, "Fresh water real-time monitoring system based on wireless sensor network and GSM," in *Proc. IEEE Conf. Open Syst.*, Sep. 2011, pp. 354–357.
[36] A. H. Sabry, W. Z. W. Hasan, M. Z. A. Kadir, M. A. M. Radzi, and S. Shafie, "Power consumption and size minimization of a wireless sensor node in automation system application," in *Proc. IEEE Regional Symp. Micro Nano Electron. (RSM)*, Aug. 2015, pp. 2–5.
[37] K. J. Singh, K. L. R. Kho, S. J. Singh, Y. C. Devi, N. B. Singh, and S. Sarkar, "Artificial neural network approach for more accurate solar cell electrical circuit model," *Int. J. Comput. Sci. Appl.*, vol. 4, no. 3, pp. 101–116, 2014.

YASMEEN HUSSEIN SABRY received the B.Sc. degree in mechanical engineering from the University of Technology-Baghdad, Iraq, in 2008. She is currently pursuing the M.Sc. degree in control and automation with the Department of Electrical and Electronic Engineering, Universiti Putra Malaysia. Her research project concerns solar-powered systems and modeling by artificial neural network.

W. Z. W. HASAN (M'07) received the degree in electrical and electronic engineering from Universiti Putra Malaysia in 1997 and the Ph.D. degree in microelectronic engineering from Universiti Kebangsaan Malaysia in 2010. He is currently a Senior Lecturer with the Department of Electrical and Electronic Engineering, Universiti Putra Malaysia. His research interests include memory testing, MEMS sensor, and robotic and automation.

A. H. SABRY received the B.Sc. degree in electrical and electronics engineering and the M.Sc. degree in control and automation engineering from the University of Technology-Baghdad, Iraq, in 1994 and 200, respectively, and the Ph.D. degree in dc-based PV-powered home energy system from the Department of Electrical and Electronic Engineering, Control and Automation, Universiti Putra Malaysia. His research project concerns integrated solar-powered smart home system based on voltage matching and dc distribution.

MOHD ZAINAL ABIDIN AB KADIR (SM'07) received the B.Eng. degree in electrical and electronic engineering from Universiti Putra Malaysia, Selangor, Malaysia, and the Ph.D. degree in high-voltage engineering from the University of Manchester, U.K. He is currently the Deputy Dean (Research & Innovation) and a Professor with the Faculty of Engineering, Universiti Putra Malaysia. He is also the Director with the Centre for Electromagnetic and Lightning Protection Research, Universiti Putra Malaysia. He is also a Professional Engineer (P.Eng.) and a Chartered Engineer (C.Eng.) and currently is the Chairman of the National Mirror Committee of TC 81 (Lightning Protection), the Chairman of MNC-CIGRE C4 on System Technical Performance, and a Working Group Member of the IEEE PES Lightning Performance on Overhead Lines, CIGRE C4.23, and CIGRE C4.27. To date, he has authored and co-authored over 300 technical papers, comprising of high impact journals, and conference proceedings. He has supervised nine Ph.D. and 24 M.Sc. students and currently 17 Ph.D. and 15 M.Sc. are on their way. His research interests include high-voltage engineering, electromagnetic compatibility, and power system transients. He is a member of IET, IEM, and CIGRE.

M. A. M. RADZI (M'07) was born in Kuala Lumpur, Malaysia, in 1978. He received the B.Eng. (Hons.) and the M.Sc. degrees from Universiti Putra Malaysia (UPM), Serdang, Selangor, Malaysia, and the Ph.D. degree from the University of Malaya in 2010. He is currently an Associate Professor with the Department of Electrical and Electronic Engineering, Faculty of Engineering, UPM, and a Researcher with the Centre for Advanced Power and Energy Research, UPM. His research interests are power electronics, power quality, and renewable energy. He is a member of the Institution of Engineering and Technology, U.K., and a Chartered Engineer.

S. SHAFIE was born in Pahang, Malaysia. He received the B.E. degree in electrical and electronics engineering from the University of the Ryukyus, Japan, in 2000, the M.E. degree in electrical and electronics engineering from the Tokyo University of Agriculture and Technology in 2005, and the Ph.D. degree in nanovision from Shizuoka University in 2008. From 2000 to 2002, he was with ALPS Electric (M) Sdn. Bhd. He is currently an Associate Professor with Universiti Putra Malaysia and the Head of the Functional Devices Laboratory. He is working in Mix Signal IC Design and Solar Energy Research. His current projects include ultra-low-power SAR ADC and high efficiency dye sensitized solar cell. He is currently the Chapter Chair of the IEEE Circuits and Systems Malaysia Chapter and actively involves in IEEE CAS and IMS Malaysia Chapters activities.